scientific reports

Check for updates

OPEN

Assessment of potato surpluses as eco-friendly adsorbent for removal of Orange II: optimization and kinetic modelling at different pH values

Diego Morales-Urrea[1]✉, Edgardo Martín Contreras[2] & Alex López-Córdoba[1]

Orange II, an azo dye used in textile and leather industries, is toxic and contributes to reducing dissolved oxygen in water. In this sense, agri-food waste adsorbents offer efficient, cost-effective dye removal. In this study, potato surpluses were evaluated as adsorbents for the removal of Orange II at 22 °C and pH values between 4 and 9. The adsorbents were characterized by their morphology, elemental composition, infrared spectra, and point of zero charge. Adsorption isotherms were analysed using Langmuir and Freundlich models, revealing that the Langmuir equation ($0.933 < r^2 > 0.882$) better described the adsorption process compared to the Freundlich model ($0.909 < r^2 > 0.852$). The maximum adsorption capacity at pH 4 was 1.1 and 2.3 times higher than at pH 7 and 9, respectively. This increased capacity at pH 4 was due to favourable electrostatic interactions between the cationic adsorbent surface and the anionic dye. A kinetic model was developed to understand the adsorption dynamics of Orange II, demonstrating high accuracy with coefficients of determination (r^2) exceeding 0.99 across various pH values. The predictions of the kinetic model aligned well with the Langmuir isotherm results, indicating a strong theoretical foundation. The critical contact time required to achieve the minimum adsorbent concentration necessary for meeting a discharge limit of 14.7 mg L^{-1} was determined using both the Langmuir and kinetic models. Simulation profiles showed that when the adsorbent concentration was increased from 12 to 40 g L^{-1}, the contact time necessary to achieve the discharge limit decreased from 26 to 3.35 h, highlighting the trade-off between contact time and cost. This study offers a cost-effective solution for wastewater treatment and presents a robust model for optimizing batch adsorption processes, marking a significant advancement in using potato surpluses for dye removal.

Keywords Adsorption, Kinetic, Optimization, Orange II, Potato, Surplus

Azo dyes, such as Orange II (OII), are widely used in various industries, including textiles and manufacturing[1]. Due to their persistence, toxicity, and carcinogenicity, azo dyes pose significant environmental and health risks[2]. These dyes can absorb light, disrupting photosynthesis in aquatic ecosystems and reducing dissolved oxygen levels[3]. With 10–15% of dyes produced globally ending up in wastewater[4], their removal is a critical concern.

Conventional wastewater treatments combine physical, chemical, and biological processes to remove pollutants[5]. However, many dyes are not fully eliminated by these methods[6], necessitating additional treatment approaches like adsorption, enzymatic catalysis, and advanced oxidation processes[5]. Among these, adsorption is particularly promising due to its high efficiency and use of non-toxic reagents compared to processes like the Fenton reaction[7]. Recent developments in adsorbent materials, including ceramics and composites, have shown efficacy in removing dyes and toxic metals from aqueous media[8–12]. However, the valorisation of agro-food waste remains a challenge for developing eco-friendly and economically viable adsorbents[13].

[1]Grupo de Investigación en Bioeconomía y Sostenibilidad Agroalimentaria, Escuela de Administración de Empresas Agropecuarias, Facultad Seccional Duitama, Universidad Pedagógica y Tecnológica de Colombia, Carrera 18 Con Calle 22, 150461 Duitama, Colombia. [2]Instituto de Investigaciones en Ciencia y Tecnología de Materiales (INTEMA), CCT-Mar del Plata, CONICET, Av. Colón 10850, 7600 Mar del Plata, Argentina. ✉email: diego.morales06@uptc.edu.co; dmoralesurrea@gmail.com

Globally, one-third of food produced for human consumption is wasted or lost, amounting to 1.3 billion tons annually[14]. This waste arises from factors such as overproduction and market influences (surplus), intentional food waste at the end of the supply chain (waste), and unintentional food loss during processing or transportation (loss)[15,16]. The management of these food wastes, often through incineration or landfilling, can lead to environmental issues such as greenhouse gas emissions and toxic leachates[17,18].

Potatoes are among the most widely cultivated tubers, with a global yield of 359 million tons in 2020 and projected production reaching 500–750 million tons by 2025 and 2030, respectively[19]. Composed of lignin, cellulose, and hemicellulose, potatoes offer physical adsorption sites for dye molecules (Stavrinou et al., 2018). While several authors have reported the utilization of potato peels (loss) for dye adsorption[20–23], there is limited research on the efficacy of potato surplus in dye removal. Potato surplus refers to tubers that have no commercial value due to factors like market conditions.

In this study, surpluses of potato were used as eco-friendly adsorbents for Orange II (OII), presenting an innovative approach to valorising agro-food waste. A kinetic model was developed to understand adsorption dynamics and optimize adsorbent use and contact time, balancing efficiency and cost. This approach is crucial for designing sustainable batch adsorption processes for treating coloured wastewater.

Materials and methods
Raw materials and reagents
The surplus of potato tubers (*Solanum tuberosum)* was kindly donated by a local market (Duitama, Boyacá, Colombia). The potato tubers used were collected according to Colombian legislation. Orange II (OII) sodium salt (96%) was acquired from Biopack (Buenos Aires, Argentina). The structure of OII and some of its chemical characteristics are shown in Table 1. The inorganic salts used for the preparation of the buffer solutions were NaH_2PO_4 (99%) and Na_2HPO_4 (99%). These salts were sourced from Loba Chemie PVT. LIDA (Maharastra, India). All methods, including experiments and analyses, were performed in accordance with relevant national and international protocols, guidelines, and regulations.

Preparation of potato surplus-based adsorbent
Figure 1 shows the schematic representation of the preparation of potato surplus-based adsorbent. The surplus of potato tubers was conditioned according to a previous work[25]. Briefly, 1 kg of tubers was peeled and cut into cubes of approximately 30 mm. Then, potato cubes were immersed in an ascorbic acid solution (1% w/v, pH 5.0) for 1 h as an anti-browning treatment. Finally, these cubes were frozen at − 20 °C for 12 h and then dried in a BUCHI Lyovapor L-200 freeze dryer (Flawil, Switzerland) operated at − 55 °C at a chamber pressure of 0.1 mbar
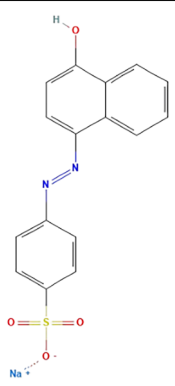
IUPAC name	Sodium 4-[(2E)-2-(2-oxonaphthalen-1-ylidene)hydrazinyl]benzenesulfonate	
CAS number	633-96-5	
Chemical formula	$C_{16}H_{11}N_2NaO_4S$ (sodium salt)	
Molar mass	350.32 g/mol	
Solubility	Very soluble in water	
Dye class	Azo	
pKa	8.26, 11.4	

Table 1. Chemical structure and general characteristics of Orange II (adapted from Sabnis, 2010).
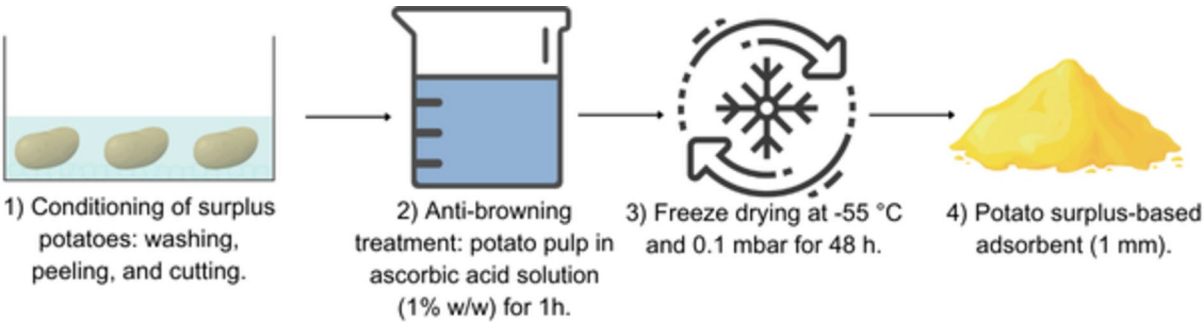

Fig. 1. Schematic representation of the preparation of potato surplus-based adsorbent.

for 48 h. The obtained potato surplus-based adsorbent (PSBA) was grounded to obtain a powder with an average diameter of 1 mm and stored in a hermetic flask until use.

Characterization of potato surplus-based adsorbent (PSBA)

Scanning electron microscopy (SEM–EDS)
The morphology of the absorbent samples was studied using a scanning electron microscope (SEM) operated at a voltage of 20 kV (Thermo Fisher Scientific, Apreo 2 S LoVac model). Elemental identification was performed using an energy dispersive X-ray spectrometry (EDS) probe (Fisher Scientific, ANAX-30P-B model).

Fourier transform infrared spectroscopy (FTIR)
FTIR analysis was performed using a Perkin-Elmer Spectrum TwoTM IR spectrometer (Waltham, MA, USA) equipped with an attenuated total reflectance (ATR) module. Infrared (IR) spectra were recorded between 4400 and 400 cm^{-1} with 20 scans and a spectral resolution of 2 cm^{-1}.

Point of zero charge (PZC) of adsorbent (PSBA)
PZC was determined using the technique proposed by Bakatula et al. (2018). 0.2 g of PSBA was mixed with 40 mL of 0.1 M $NaNO_3$ solutions at initial different pH values ($pH_i = 3–9$). Then, these mixtures were stirred at 150 rpm for 24 h and the final pH values (pH_f) were measured. The pH_{pzc} was determined as the point of intersection where the pH_i versus ΔpH ($pH_f–pH_i$) plot intersects with $\Delta pH = 0$. All determinations were performed in duplicate.

Orange II (OII) adsorption assays

The capability of PSBA to remove OII was tested according to a previous work[25]. Adsorption assays were performed by mixing OII solutions (7–525 mg L^{-1}) with PSBA suspensions (3.8–7.6 g L^{-1}) at pH values ranging from 4 to 9 until the equilibrium was achieved (Fig. 2). The temperature of the test was controlled at 22 °C (INGELAB, I-122PF). All determinations were performed in duplicate. At predetermined intervals, 2 mL from the reaction mixture were centrifuged for 20 min at 5000 rpm (Benchmark Scientific, MYFUGE 12) to remove the PSBA. Then, the absorbance of the supernatant was measured at 485 nm in a spectrophotometer X-ma 1200 (Human Corporation, Loughborough, UK). The OII concentration in the supernatant was calculated using a molar attenuation coefficient of 19.6 ± 0.2 a.u. mM^{-1} cm^{-1}[27]. Finally, the OII concentration was converted from mmol L^{-1} to mg L^{-1} using the corresponding molecular weight (Table 1).

Once the equilibrium between aqueous and adsorbed OII was reached, the equilibrium adsorption capacity of OII onto PSBA (q_e, mg g^{-1}) was calculated as follows:

$$q_e = \frac{C_0 - C_e}{[PSBA]} \tag{1}$$

where C_0 and C_e (mg L^{-1}) are the initial and equilibrium OII concentrations, respectively, and [PSBA] (g L^{-1}) is the tested PSBA concentration. Note that the term $C_0 - C_e$ represents the amount of OII adsorbed per unit volume of the liquid phase.

Langmuir (Eq. 2) and Freundlich (Eq. 3) models were fitted to equilibrium adsorption capacity (q_e) as a function of the equilibrium OII concentration (C_e):[28]

$$q_e = q_m \frac{C_e}{K_L + C_e} \tag{2}$$

$$q_e = K_F C_e^{1/n} \tag{3}$$

- Adsorbent concentration: 3.8 - 7.6 g L^{-1}
- OII concentration: 7 - 525 mg L^{-1}
- pH: 4 - 9
- Temperature: 22 °C

Orange II solution (OII)

Potato surplus-based adsorbent (PSBA)
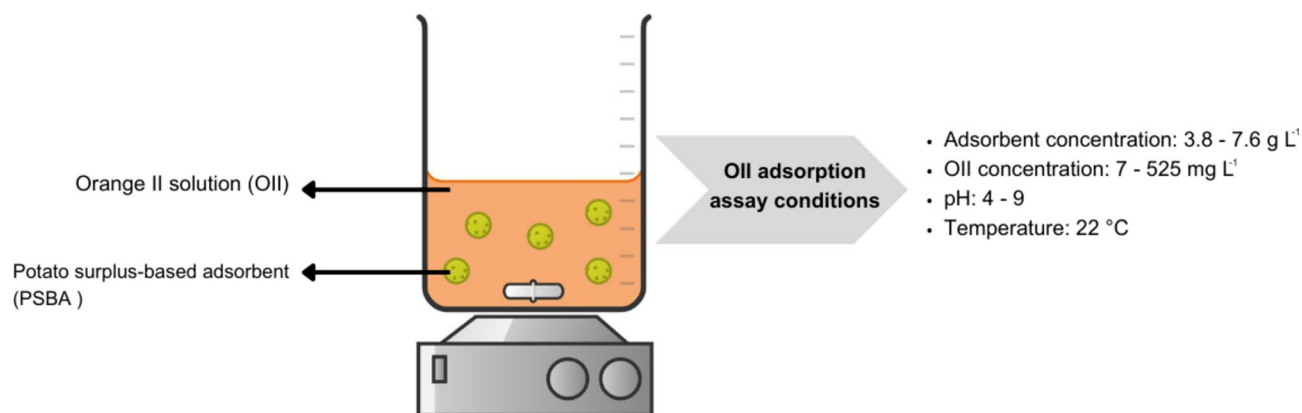
OII adsorption assay conditions

Fig. 2. Schematic representation of the adsorption assays of Orange II solutions (OII).

where q_m (mg g^{-1}) is the maximum adsorption capacity of the tested adsorbent, K_L (mg L^{-1}) is the semisaturation constant, and K_F and n are the constants corresponding to the Freundlich adsorption isotherm.

Ethical approval

No manipulation of human or animal tissue was performed in this work. The tubers used were collected according to Colombian protocols, guidelines, and regulations.

Results and discussion

Microstructure analysis of adsorbent

Figure 3 shows the microstructure of the adsorbent before (Fig. 3a) and after (Fig. 3b) being used for the removal of Orange II. In general, the microstructure of the starch is observed in spherical and oval. Also, no pores were observed in the images, suggesting that the material is not naturally porous.

Table 2 shows the EDS elemental analysis of the adsorbent before and after OII removal assays. The predominant elements in the adsorbent were carbon (46.5% w/w) and oxygen (46.6% w/w). Bouhadjra et al.[20] reported similar results in potato peels. These carbon and oxygen compositions are associated with the cellulose, hemicellulose, and lignin in potatoes[23]. Additionally, a significant increase in oxygen, sodium, and nitrogen was observed post-adsorption. Orange II (Table 1) likely contributed to these increased levels, but the rise in potassium, sodium, and oxygen could also be due to the use of sodium phosphate salts as buffer solutions.

FTIR analysis of adsorbent

Figure 4 shows the FTIR spectrum of the adsorbent before and after the OII adsorption assays. The adsorbent exhibited characteristic absorption bands at 1733 cm^{-1}, corresponding to C=O bonds, and at 1637 cm^{-1}, associated with C=C vibrations of polyphenolic compounds[20,23]. The IR spectrum also showed characteristic bands at 2911 cm^{-1} (C–H$_2$ asymmetric stretching) and 3266 cm^{-1} (O–H stretching), indicating the presence of methoxyl groups in cellulose, hemicellulose, and lignin. Figure 4 (inset) also shows changes in the FTIR spectrum after the OII adsorption assays. New bands at 1284 cm^{-1} and 1459 cm^{-1} correspond to symmetric stretching vibrations of S(=O)$_2$ in the group -SO$_3^{2-}$ group and the stretching vibration of –N=N–, respectively[29,30]. Jin et al. (2014), observed these peaks during FTIR analysis of OII, while Kali et al.[30], identified these bands after the adsorption of an azo dye on almond shells. It must be mentioned that after the OII removal assays, the adsorbent
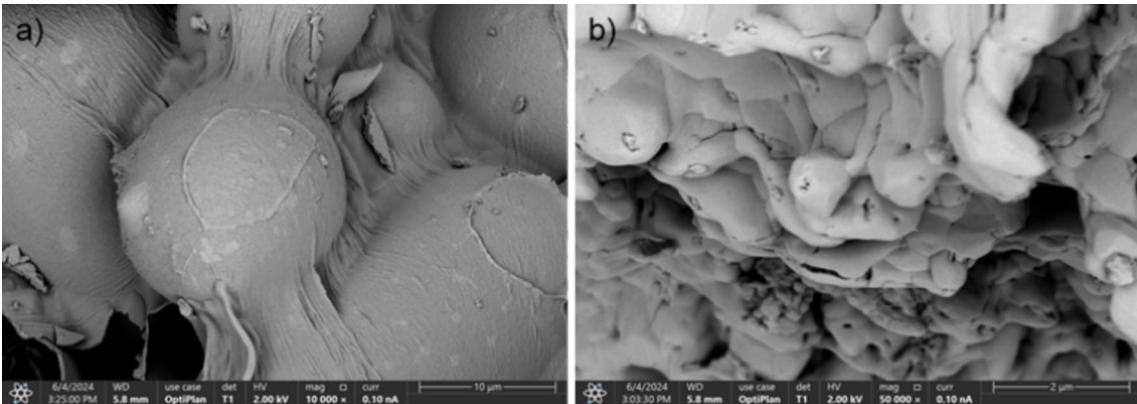

Fig. 3. Microstructure of the adsorbent before (**a**) and after (**b**) being used for the removal of Orange II.

Element	Adsorbent		Adsorbent post-OII removal	
	Atomic (%)	Weight (%)	Atomic (%)	Weight (%)
Carbon	55.5	46.5	22.8	46.5
Nitrogen	0.0	0.0	3.9	0.0
Oxygen	41.8	46.6	52.5	46.6
Sodium	0.0	0.1	11.6	0.1
Magnesium	0.3	0.5	0.0	0.5
Phosphorus	0.1	0.3	8.9	0.3
Sulfur	0.2	0.4	0.0	0.4
Chlorine	0.1	0.2	n.d	0.2
Potassium	2.0	5.4	0.3	5.4

Table 2. EDS elemental analysis of the adsorbent before and after Orange II removal. n.d = not detected.
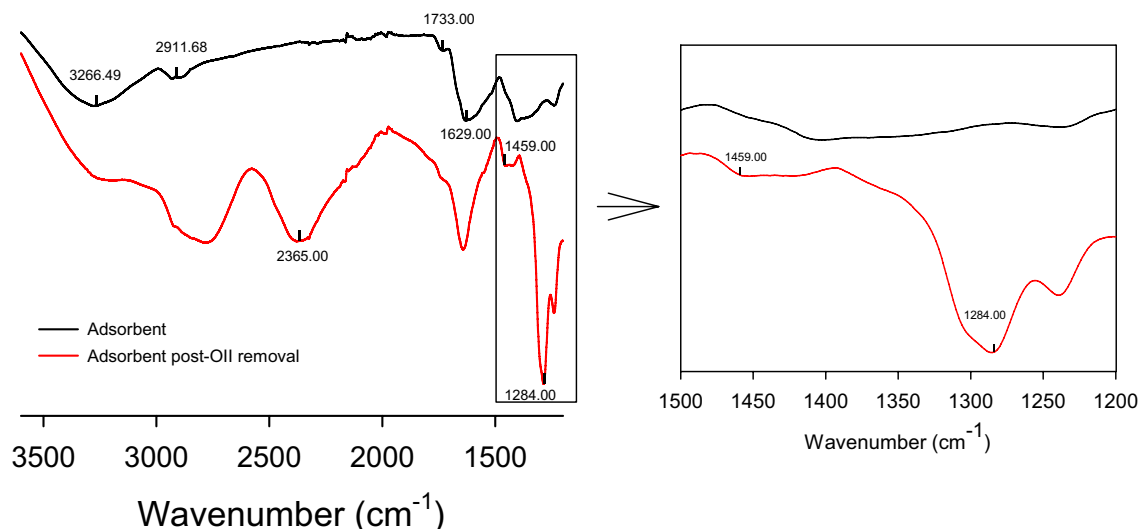
Fig. 4. FTIR spectra of adsorbent before (black line) and after (red line) the Orange II (OII) removal assays. The inset shows a detail of the spectra before (black line) and after (red line) the OII removal assays, highlighting the new peaks at 1459 cm^{-1} and 1284 cm^{-1} due to dye adsorption.

was colored orange. Considering that O–H moieties are known active sites for the adsorption of organic dyes[23], this result suggests that the adsorbent is effective for OII removal.

Point of zero charge (PZC) of adsorbent

By definition, the point of zero charge (PZC) of a material is the pH value at which the surface charge of the tested material is zero under a given experimental condition (Bakatula et al.[26]). At this point, both positive and negative surface charges are equal. In principle, at pH values higher than the PZC, the adsorbent surface has a net negative charge. Conversely, the solid surface is positively charged in the cases when pH is lower than the PZC. Figure 5 shows the experimental curve of ΔpH as a function of pH_i corresponding to PSBA. The PZC of adsorbent (PSBA) was identified at pH = 4.7 ± 0.2. Hence, the PSBA surface will exhibit positive and negative global charges at pH values below and above pH = 4.7, respectively. The obtained PZC value was lower than those reported by Jeddou et al.[21], and Stavrinou et al.[23] for potato peels (about 6). However, it must be noted that in the present work, pulp instead of potato peels was studied.

OII adsorption assays

Figure 6 shows the effect of the initial concentrations of adsorbent ([PSBA], g L^{-1}) and orange II(OII, mg L^{-1}) on dye removal (R_{OII}, %) at pH 4. When the adsorbent concentration was doubled, the R_{OII} values increased by approximately 1.4-fold. This behaviour was attributed to an increase in surface area and the number of available active sites for dye adsorption[30,31]. Additionally, the R_{OII} values increased with adsorbate concentrations, reaching a maximum at around 25 mg L^{-1}. Beyond this concentration, a noticeable decrease in R_{OII} values was observed, likely due to the saturation of the PSBA surface by OII molecules. This behaviour has been previously reported by several authors[21,23].
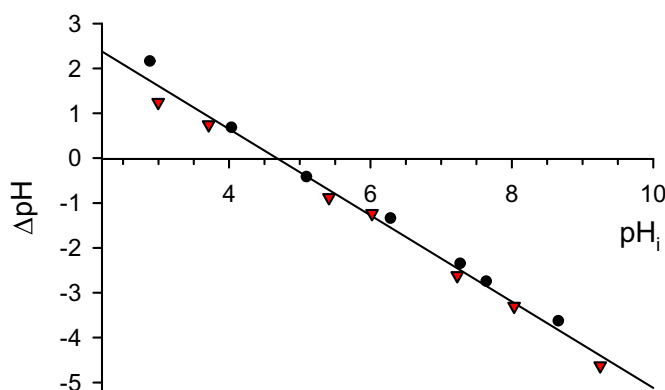

Fig. 5. PZC determination of adsorbent (PSBA). Different symbols indicate independent experiments, line represents the linear regression (r^2 = 0.9891).
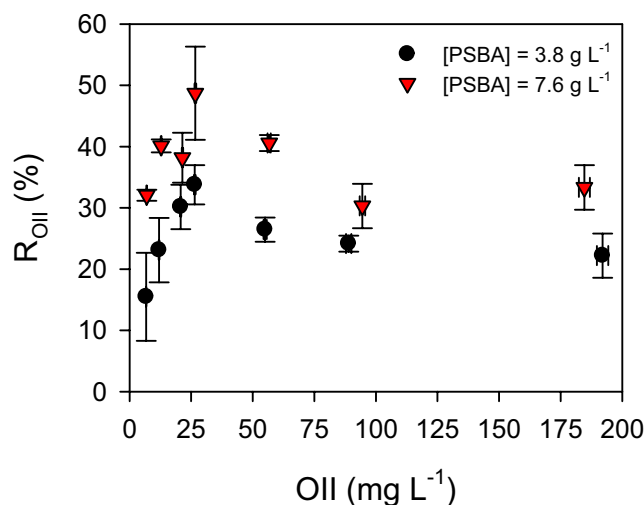
Fig. 6. Effect of the initial concentrations of adsorbent ([PSBA], g/L) and dye (OII, mg L^{-1}) on the OII removal (R_{OII}, %) at pH4. Barr lines indicate the standard deviation.

Before performing an equilibrium adsorption isotherm, it is crucial to evaluate the time necessary to achieve equilibrium. Figure 7 shows examples of OII adsorption onto PSBA as a function of time at different initial pH values. Kinetic assays demonstrated that in all cases, adsorption equilibrium was reached within the tested time interval. Equilibrium conditions were attained after at least 48 h, regardless of the tested pH. Under the experimental conditions in Fig. 7, the maximum OII removals at pH 4, 7, and 9 were 38%, 12%, and 18%, respectively. These results suggest that low pH values favour the adsorption of OII onto PSBA.

As a general rule, pH is a key factor that strongly affects the maximum adsorption capacity (q_m) of natural adsorbents[20,26]. Because the change in adsorption capacity as a function of pH depends on both the adsorbate and the adsorbent, it is crucial to evaluate the effect of pH on the adsorption process of new materials such as PSBA. Figure 8 shows the equilibrium adsorption isotherms of OII onto PSBA at the tested pH values. As a general trend, the adsorption capacity (q_e) increased with the equilibrium concentration of OII (C_e), reaching a plateau that varied with pH.

Langmuir (Eq. 2) and Freundlich (Eq. 3) models were fitted to the data presented in Fig. 8. According to the coefficients of determination (r^2) shown in Table 3, the adsorption isotherms are more accurately described by the Langmuir equation (Eq. 2) than by the Freundlich model (Eq. 3) within the tested pH range. The maximum adsorption capacities were determined to be 21.4 ± 1.8 mg g^{-1} (Langmuir) and 0.54 ± 0.13 mg g^{-1} (mg L^{-1})$^{-1/n}$ (Freundlich). Table 4 compares these values with those reported in the literature for dyes adsorption using waste and loss of potato. Notably, these studies employed adsorbent powders derived from potato peels, leaves, and stems through dehydration at temperatures near 100 °C, whereas the current study used lyophilized pulp from potato surpluses. Table 4 shows that, except for methylene blue, the maximum adsorption capacities for these adsorbents generally align with the range observed in this study. The discrepancy for methylene blue may be attributed to its smaller molecular size compared to the other dyes.

From the data presented in Table 3, it was calculated that the maximum adsorption capacity (q_m) of the PSBA at pH = 4 was only 1.1 and 2.3 times higher than at pH = 7 and 9, respectively. Despite this, the main difference occurred at low OII equilibrium concentrations (C_e), as seen in Fig. 8. In this context, azo dyes such as Orange II typically exhibit a broad absorption band within the visible spectrum[32]. Generally, these dyes have maximum molar attenuation coefficients ranging from 1.6 (methyl red) to 182 (p-ethoxychrysoidine) a.u. mM^{-1} cm^{-1}[33,34]. Consequently, even relatively low concentrations of azo dyes can produce colored wastewater with high absorbance values. Furthermore, adsorption processes are often employed as a final step in effluent polishing to reduce specific pollutants to very low concentrations. This implies that such adsorption processes generally operate within a low concentration range[35,36]. Under these conditions, calculations demonstrate that the adsorption of OII by PSBA is significantly favored at pH = 4 compared to higher pH values. Several studies have reported similar findings regarding the effect of pH on the adsorption capacity of dyes onto potato peels and leaves[20,21,23,31].

Considering that the PZC corresponding to PSBA is 4.7 (Fig. 5), the maximum value of q_m was obtained when the solid surface was positively charged (pH 4). Conversely, results demonstrate that at pH values higher than PZC, the adsorption of OII was not favoured by the negatively charged PSBA surface. A similar trend has been reported by Jeddou et al.[21] and Stavrinou et al.[23] during the adsorption of anionic dyes on potato peel at room temperature. At this point, it is worth mentioning that OII is a diprotic acid with pKa1 = 8.26, and pKa2 = 11.4 (Table 1), corresponding to the deprotonation of the –SO$_3$H moiety of the benzene ring, and the –OH of the naphthalene ring, respectively[24,37]. Using these pKa values, the fraction corresponding to each dye species as a function of pH can be calculated (Supporting Information, Item 1). According to Fig. S1, for pH values lower than 6 the undissociated OII was the main dye species (99.99%). Then, the monovalent form of OII increases as a function of the pH. However, at pH = 7, the undissociated fraction is still higher than the monovalent species,
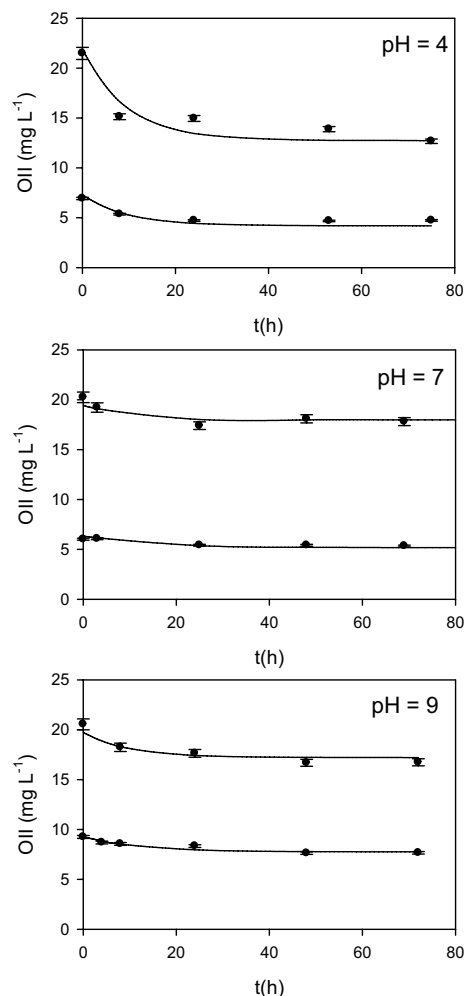
Fig. 7. Typical examples corresponding to the adsorption of Orange II (OII, mg L^{-1}) onto adsorbent (7.58 g L^{-1}) as a function of time at different initial pH values. In all cases, bars represent the standard deviation, and lines correspond to the proposed model (Eqs. 4–6) using the coefficients shown in Table 5.

being for 95%, and 5%, respectively. The monovalent OII species becomes the main form of OII when the pH value increases to 9. In this case, undissociated and monovalent species are about 15%, and 85%, respectively. Thus, within the tested pH range in the present work (4–9), undissociated or monovalent OII are the dominant species. Considering that the highest q_m value was obtained at pH = 4 (Fig. 8, Table 3) and then, q_m decreased for higher pH values, the low OII adsorption capacity of pH values above the PZC of the PSBA could be due to the result of the electrostatic repulsion between the monovalent form of OII and the negatively charged surface of the PSBA.

Modelling the adsorption kinetics of Orange II (OII) onto adsorbent (PSBA)

In order to select the best operating conditions in full-scale batch processes, the knowledge of the adsorption kinetics of a given adsorbate onto an adsorbent is crucial. Several kinetic models, such as pseudo-first and pseudo-second-order, Weber–Moris, and Elovich, are available in the literature. Among these models, the pseudo-first and the pseudo-second-order kinetic equations are the most used ones[38]. It is important to note that these semi-empirical models focused attention on the evolution of the adsorption capacity (q) instead of the aqueous adsorbate concentration as a function of time. Unfortunately, in most cases, the conciliation between these models and the experimental adsorption equilibrium isotherm cannot be achieved. For example, pseudo-first and pseudo-second-order models contain two coefficients, a kinetic constant, and an asymptotic q value that represents the adsorption capacity at long contact times (e.g., the equilibrium condition). As a general rule, these coefficients strongly depend on the tested initial conditions. Furthermore, in most cases, there is no theoretical link between these kinetic coefficients and the experimental adsorption equilibrium isotherm.

In the present work, the adsorption kinetics was represented by the model proposed by Ferro Orozco et al. (2010). According to several authors, the total concentration of adsorption sites (TS) is proportional to the adsorbent concentration[30,31]. In the present model, α (mmol g^{-1}) represents the proportionality constant between the amount of the adsorbent (PSBA in this work) and adsorption sites. To simplify the model, Ferro Orozco et al.[39] assumed that all adsorption sites are equal and independent of each other. Thus, the occupation of a free
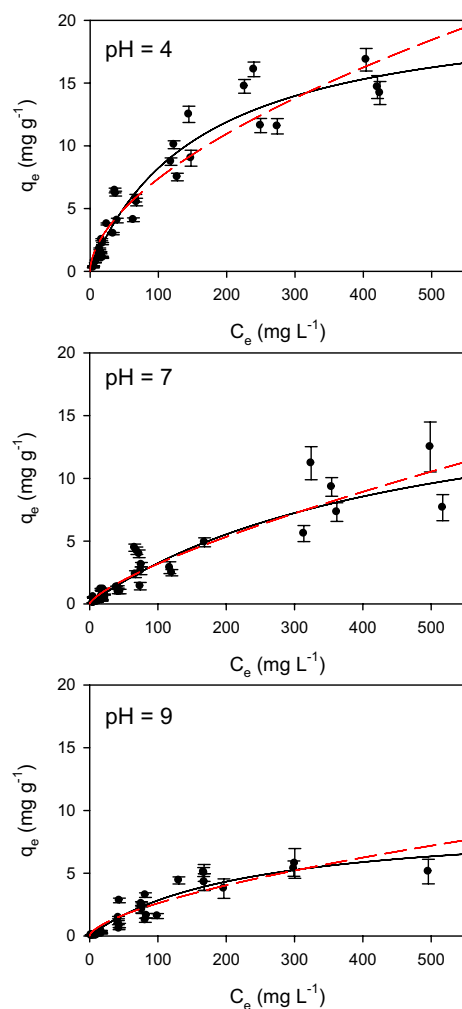
Fig. 8. Equilibrium adsorption isotherms of Orange II onto adsorbent at different pHs. Bars indicate the standard deviation. Continuous lines represent the Langmuir model (Eq. 2), dashed lines correspond to the Freundlich model (Eq. 3). Fitting results are shown in Table 3.

Model	Coefficient	pH = 4	pH = 7	pH = 9
Langmuir	q_m (mg g^{-1})	21.4 ± 1.8	19.6 ± 4.2	9.1 ± 1.4
	K_L (mg L^{-1})	161 ± 31	476 ± 165	220 ± 59
	r^2	0.9336	0.8825	0.8991
Freundlich	K_F (mg g^{-1} (mg L^{-1})$^{-1/n}$)	0.54 ± 0.13	0.11 ± 0.04	0.14 ± 0.05
	n	1.76 ± 0.14	1.35 ± 0.11	1.59 ± 0.16
	r^2	0.9094	0.8769	0.8525

Table 3. Results corresponding to the fit of Langmuir (Eq. 2) and Freundlich (Eq. 3) models to the data shown in Fig. 8.

site does not affect other sites. Accordingly, a free adsorption site (FS) can be occupied by an adsorbate molecule to produce an occupied site (OS):

$$C + FS \underset{k_d}{\overset{k_a}{\rightleftarrows}} OS \tag{4}$$

Adsorbent	pH	Dye	Molecular weight (g mol⁻¹)	Langmuir model (mg.g⁻¹)	Freundlich model (mg g⁻¹ (mg L⁻¹)⁻¹ᐟⁿ)	References
Potato stem powder	7	Methylene blue	319.90	41.60	2.27	31
Potato stem powder	7	Malachite green	364.91	27.00	1.45	31
Potato leaves powder	7	Methylene blue	319.90	52.60	3.15	31
Potato leaves powder	7	Malachite green	364.911	33.30	2.06	31
Potatoes peels	2	Orange g	452.38	23.60	5.66	23
Potatoes peels	9	Methylene blue	319.9	107.40	14.94	23
Potatoes peels	6	Methylene blue	319.9	97.08	0.46	21
Potatoes peels	2	Direct red 80	1373.1	27.77	2.38	21
Pulp of potato surplus	4	Orange II	350.32	21.40	0.54	This work

Table 4. Comparison of the highest adsorption capacity values reported in the literature using waste, loss, and surplus of potato as dyes adsorbents.

where C represents the adsorbate (e.g., OII), FS and OS are free and occupied adsorption sites, and k_a (mM⁻¹ h⁻¹) and k_d (h⁻¹) are the adsorption and desorption kinetic constants, respectively. Besides, for a given concentration of the adsorbent (PSBA in this work), the balance of adsorption sites is as follows:

$$[TS] = \alpha[PSBA] = [FS] + [OS] \tag{5}$$

According to Eq. (4), rates corresponding to C, FS, and OS are as follows:

$$\frac{d[C]}{dt} = \frac{d[FS]}{dt} = -\frac{d[OS]}{dt} = -k_a[C][FS] + k_d[OS] \tag{6}$$

It is important to note that the equalities represented by Eq. (6) are valid only if the variables are expressed in mol but not in weight. For this reason, the use of mol-based units instead of weights to express concentrations facilitates the development of kinetic models.

By definition, the adsorption equilibrium occurs when adsorption and desorption rates are equal:

$$k_a C_e [FS]_e = k_d [OS]_e \tag{7}$$

where the subindex e refers to the equilibrium condition. Then, combining eqs.(6) and (7), the following expression can be obtained:

$$\frac{[OS]_e}{[PSBA]} = \alpha \frac{C_e}{\left(\frac{k_d}{k_a}\right) + C_e} \tag{8}$$

The term $\frac{[OS]_e}{[PSBA]}$ (mmol g⁻¹) represents the amount of OII adsorbed (mmol) per unit mass (g) of PSBA in equilibrium with the aqueous phase OII concentration (C_e). Considering that Eqs. (2) and (8) represent the equilibrium between adsorption between the adsorbent (PSBA) and the adsorbate (OII), from the comparison between Eqs. (2) and (8), it can be concluded that $\frac{[OS]_e}{[PSBA]} = q_e, \alpha = q_m$, and $\frac{k_d}{k_a} = K_L$. Thus, Eq. (8) demonstrates that the Langmuir equation (Eq. 2) can be derived from the kinetic model proposed by Ferro Orozco et al.[39]. Moreover, these relations are very useful for reducing the number of parameters to fit. In particular, because Langmuir coefficients were known (Table 3), using the above-mentioned relations, only one parameter of the model (k_a in this work) is necessary to fit. This approach ensures compatibility between the fitting results of the Langmuir equation with the results obtained by fitting the tested kinetic model to the change in the OII concentration as a function of time.

The kinetic model (Eqs. 4–6) was fitted to the experimental data (OII concentration as a function of time for different initial OII and PSBA concentrations) at the three tested pH values using the software package Gepasi 3.30[40]. To integrate the system of differential equations, the routine LSODA (Livermore Solver of Ordinary Differential Equations) was selected. Briefly, the LSODA algorithm measures the stiffness of the equations and switches the integration method dynamically according to this measure. For non-stiff regions, the Adams integration method with variable step size and variable order up to 12th order is used; for stiff regions the Gear (or BDF) method with variable step size and variable order up to 5th order is used. Additionally, the Multistart Optimization algorithm (with Levenberg–Marquardt local optimization) was selected as the optimization method. Multistart is a hybrid stochastic–deterministic optimization method that runs several simple local optimizations using the gradient descent method, each time starting from a different initial guess. While the first start takes for initial guess of the parameter values entered by the user, subsequent starts are generated randomly within the boundaries for the adjustable parameters selected by the user. According to Mendes & Kell[41], the Multistart Levenberg–Marquardt method is one of the most efficient gradient optimizers among the available ones in Gepasi.

Fitting results corresponding to the tested kinetic model (Eqs. 4–6) are shown in Table 5. As a general rule, a satisfactory agreement between experimental and model data was obtained (Fig. 5; Fig. 9, left panel). For all the tested pH, coefficients of determination (r^2) were higher than 0.99 (Table 5). Moreover, Fig. 9 (right panel)

pH	α^* (mmol g^{-1})	K_L^* (mM)	k_a (mM^{-1} h^{-1})	$k_d = K_L k_a$ (h^{-1})	r^2	N**
4	0.061 ± 0.005	0.46 ± 0.09	0.123 ± 0.035	0.057 ± 0.020	0.9931	127
7	0.056 ± 0.012	1.36 ± 0.47	0.012 ± 0.002	0.016 ± 0.006	0.9973	97
9	0.026 ± 0.004	0.63 ± 0.17	0.079 ± 0.008	0.050 ± 0.005	0.9994	120

Table 5. Fitting results corresponding to the tested kinetic model (Eqs. 4–6). *Adopted from the Langmuir model (Table 3) using the molecular weight of OII (Table 1). **Total number of experimental data.

Fig. 9. Parity plots (left panel) between experimental data and the adsorption kinetic model (Eqs. 4–6), and cumulative distribution of absolute fitting errors (right panel). Continuous lines represent the perfect correlation. Dashed lines correspond to a cumulative probability of 50%.

demonstrates that 50% of the simulated data had absolute errors less than 0.006 mM for all the tested pH values. Table 5 also showed a strong decrease of k_a for pH values higher than 4. This behaviour is in accordance with the above-mentioned electrostatic repulsion effect between the negatively charged PSBA surface at pH values above the PZC, and the OII monovalent anionic species (see Sect. "OII adsorption assays").

Adsorption processes are often used as a final polishing step to meet discharge criteria of certain compounds, such as azo dyes, that could not be fully removed by conventional methods[35,42,43]. In the case of textile wastewater, the main problem is the high and unnatural color due to the presence of dyes after the treatment[44]. Once a given adsorbent is selected, the key point in designing a batch adsorption process is to estimate the adsorbent concentration (PSBA in this work) necessary to meet a certain effluent discharge limit. For example, the true colour (e.g., the colour after removing suspended solids and turbidity) discharge limit in Taiwan is 400 ADMI units[44], while in India is 150 ADMI units[45]. These discharge limits correspond to maximum OII concentrations (C_L) of 0.042 (14.7 mg L^{-1}), and 0.016 mM (5.6 mg L^{-1}), respectively. Details concerning the transformation of OII concentrations to ADMI units can be found in Supplementary Information, Item 2.

Suppose you want to design a batch adsorption process as the final polishing process for a certain wastewater, for example. For long contact times, adsorbate and adsorbent eventually will reach the adsorption equilibrium. So, the aqueous concentration of the adsorbate (OII in this work) represents the outlet concentration of OII of this adsorption system. Assuming that the discharge limit (C_L) represents the concentration of dye in equilibrium with the adsorbent, the minimum concentration of the adsorbent ($[PSBA]_{min}$) necessary to meet the discharge limit can be calculated as a function of the initial (e.g., wastewater) OII concentration (C_0) by combining and rearranging Eqs. (1) and (2) as follows:

$$[PSBA]_{min} = \frac{(C_0 - C_L)(K_L - C_L)}{q_m C_L} \tag{9}$$

For example, considering a wastewater containing 0.1 mM of OII (35 mg L^{-1}) at pH = 4, and assuming a discharge limit of 400 ADMI units (OII = 0.042 mM = 14.7 mg L^{-1}), according to Eq. (9) the concentration of PSBA to reach the discharge limit is 11.37 g L^{-1}. However, it is important to note that equilibrium conditions were assumed in Eq. (9). Accordingly, this assumption implies an infinite contact time between the adsorbent and the solution to be treated, which is not technically feasible. In fact, due to kinetic restrictions, the adsorbent concentration necessary to achieve the discharge limit within a practical contact time must be higher than the calculated one employing Eq. (9). In this sense, for a given adsorbent concentration, the kinetic model used in this work (Eqs. 4–6) can be employed to obtain the critical contact time (t_C) necessary to attain the discharge limit. Figure 10a shows some simulated OII profiles as a function of time corresponding to different PSBA concentrations. From the intersection between these curves and the assumed discharge limit (dashed line in Fig. 10a), t_C values as a function of PSBA concentrations can be obtained. Figure 10b demonstrates that as PSBA decreases to the minimum PSBA concentration obtained by Eq. (9) (dashed line in Fig. 10b), t_C increases and tends to infinity, which represents the equilibrium condition. Conversely, the higher the PSBA, the lower the t_C. For example, when the PSBA concentration is increased from 12 to 40 g L^{-1}, the contact time necessary to achieve the discharge limit decreases from 26 to 3.35 h. Although lower contact times either represent smaller adsorption tanks or a higher treatment capacity, it must be noted that higher PSBA concentrations also increase the cost associated with the adsorbent. In this sense, the availability of a low-cost adsorbent, such as PSBA, favours the selection of a high adsorbent concentration, reducing the cost associated with higher adsorption tanks, for example. However, it must be noted that the optimum solution depends on many factors, such as land availability and cost, primary and secondary treatments, wastewater characteristics, inlet dye concentration, type of dye, local discharge limits, and others. In this sense, the adsorption model used in the present work can be useful for designers to find the most suitable solution for each particular case.

Conclusions

This study evaluated the use of potato surpluses as adsorbents for the removal of Orange II from aqueous media. Characterization of the adsorbents confirmed effective Orange II adsorption. The results indicated that the Langmuir model provided a better fit than the Freundlich model. The maximum adsorption capacity was significantly higher at pH 4, attributed to favourable electrostatic interactions between the cationic adsorbent surface and the anionic dye. The developed kinetic model demonstrated high accuracy, aligning well with Langmuir isotherm results and providing a strong theoretical foundation for predicting adsorption kinetics. The critical contact time required to achieve the minimum adsorbent concentration for a discharge limit of 14.7 mg/L was determined, with simulation profiles revealing that contact times decreased as the adsorbent concentration was increased from 12 to 40 g L^{-1}. This study offers a cost-effective and environmentally sustainable solution for wastewater treatment, advancing the use of potato surpluses in dye removal processes and optimizing batch adsorption processes to meet discharge criteria for coloured wastewater.
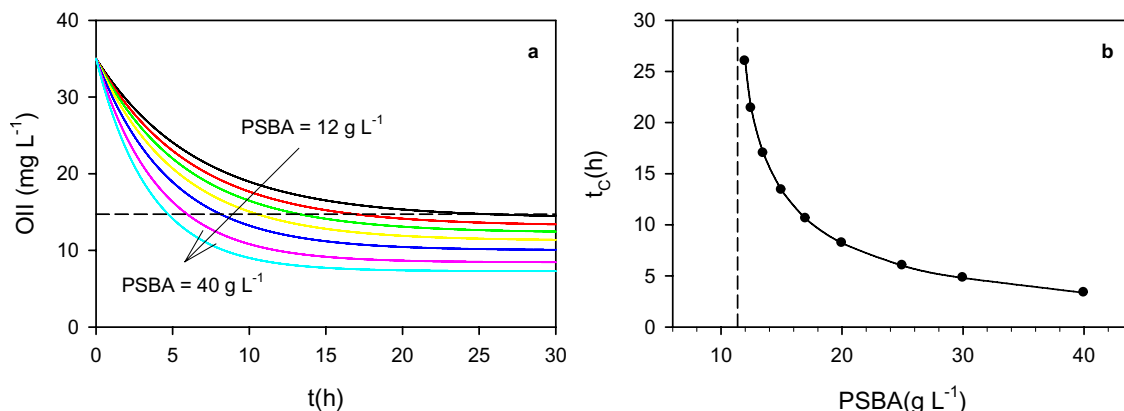

Fig. 10. (**a**) Simulated Orange II (OII) profiles as a function of time, and b) critical time necessary to achieve a discharge limit of 400 ADMI units (14.7 mg L^{-1} of OII, dashed line in a) for different adsorbent concentrations (PSBA). Dashed line in (**b**) represents the minimum PSBA concentration to achieve the discharge limit (Eq. 9). For all simulations, coefficients corresponding to pH = 4 (Table 5) were used.

Data availability
The authors declare that the data supporting the findings of this study are available within the paper and its Supplementary Information files. Should any raw data files be needed in another format they are available from the corresponding author upon reasonable request.

References
1. Yılmazoğlu, M., Turan, B., Demircivi, P. & Hızal, J. Synthesis and characterization of imidazolium based ionic liquid modified montmorillonite for the adsorption of Orange II dye: Effect of chain length. *J. Mol. Struct.* **1249**, 131628 (2022).
2. Ikram, M. *et al.* Bacillus subtilis: As an efficient bacterial strain for the reclamation of water loaded with textile azo dye, Orange II. *Int. J. Mol. Sci.* **23**, 10637 (2022).
3. Sagadevan, S. *et al.* Photocatalytic efficiency of titanium dioxide for dyes and heavy metals removal from wastewater. *Bull. Chem. React. Eng. Catal.* **17**, 430–450 (2022).
4. Haque, A. N. M. A., Sultana, N., Sayem, A. S. M. & Smriti, S. A. Sustainable adsorbents from plant-derived agricultural wastes for anionic dye removal: A review. *Sustainability* **14**, 11098 (2022).
5. Crini, G. & Lichtfouse, E. Advantages and disadvantages of techniques used for wastewater treatment. *Environ. Chem. Lett.* **17**, 145–155. https://doi.org/10.1007/s10311-018-0785-9 (2019).
6. Deng, F. & Brillas, E. Advances in the decontamination of wastewaters with synthetic organic dyes by electrochemical Fenton-based processes. *Sep. Purif. Technol.* **316**, 123764 (2023).
7. Saravanan, A. *et al.* Effective water/wastewater treatment methodologies for toxic pollutants removal: Processes and applications towards sustainable development. *Chemosphere* **280**, 130595 (2021).
8. Akkari, I. *et al.* Recycling waste by manufacturing biomaterial for environmental engineering: Application to dye removal. *Biocatal. Agric. Biotechnol.* **50**, 102709 (2023).
9. Cao, Y., Khan, A., Kurniawan, T. A., Soltani, R. & Albadarin, A. B. Synthesis of hierarchical micro-mesoporous LDH/MOF nanocomposite with in situ growth of UiO-66-(NH2)2 MOF on the functionalized NiCo-LDH ultrathin sheets and its application for thallium (I) removal. *J. Mol. Liq.* **336**, 116189 (2021).
10. Soltani, R., Marjani, A. & Shirazian, S. A hierarchical LDH/MOF nanocomposite: single, simultaneous and consecutive adsorption of a reactive dye and Cr(<scp>vi</scp>). *Dalton Trans.* **49**, 5323–5335 (2020).
11. Soltani, R. *et al.* Bio-based 3D dendritic silica nanosphere: A green superior adsorbent. *J. Clean. Prod.* **335**, 130204 (2022).
12. Soltani, R. *et al.* Synthesis of multi-organo-functionalized fibrous silica KCC-1 for highly efficient adsorption of acid fuchsine and acid orange II from aqueous solution. *Sci. Rep.* **11**, 2716 (2021).
13. Graba, Z., Akkari, I., Bezzi, N. & Kaci, M. M. Valorization of olive–pomace as a green sorbent to remove basic red 46 (BR46) dye from aqueous solution. *Biomass Convers. Biorefin.* **14**, 14951–14962 (2024).
14. Food and Agriculture Organization of the United Nations. Global Food Losses and Food Waste—Extent, Causes and Prevention. 1–37. https://www.fao.org/sustainable-food-value-chains/library/details/en/c/266053/ (2011).
15. Huang, C. H., Liu, S. M. & Hsu, N. Y. Understanding global food surplus and food waste to tackle economic and environmental sustainability. *Sustainability* **12**, 2892 (2020).
16. Rodrigues, J. P. B. *et al.* Agri-food surplus, waste and loss as sustainable biobased ingredients: A review. *Molecules* **27**, 5200 (2022).
17. Cabrera, F. C. Eco-friendly polymer composites: A review of suitable methods for waste management. *Polym. Compos.* **42**, 2653–2677 (2021).
18. Rajmohan, K., Ramya, C. & Varjani, S. Trends and advances in bioenergy production and sustainable solid waste management. *Energy Environ.* **32**, 1059–1085 (2021).
19. Food and Agriculture Organization of the United Nations. Doubling global potato production in 10 years is possible. https://www.fao.org/newsroom/detail/doubling-global-potato-production-in-10-years-is-possible/en (2022).
20. Bouhadjra, K., Lemlikchi, W., Ferhati, A. & Mignard, S. Enhancing removal efficiency of anionic dye (Cibacron blue) using waste potato peels powder. *Sci. Rep.* **11**, 2090 (2021).
21. Jeddou, K. B. *et al.* Adsorptive removal of direct red 80 and methylene blue from aqueous solution by potato peels: A comparison of anionic and cationic dyes. *Water Sci. Technol.* **83**, 1384–1398 (2021).
22. Miada, B., Bencheikh-Lehocine, M., Arris, S. & Abdeslam-Hassen, M. Adsorption removal of eriochrome black t (Ebt) and rose bengal (rb) from aqueous solutions using bio-sorbents combination. *Chem. Chem. Technol* **15**, 299–311 (2021).
23. Stavrinou, A., Aggelopoulos, C. A. & Tsakiroglou, C. D. Exploring the adsorption mechanisms of cationic and anionic dyes onto agricultural waste peels of banana, cucumber and potato: Adsorption kinetics and equilibrium isotherms as a tool. *J. Environ. Chem. Eng.* **6**, 6958–6970 (2018).
24. Sabnis, R. W. *Handbook of Biological Dyes and Stains* (Wiley, Hoboken, 2010).
25. Morales-Urrea, D. A., López-Córdoba, A. F. & Contreras, E. M. Uso de la pulpa de papa como biomaterial para la remoción de un contaminante industrial (Orange II). *Información Tecnológica* **33**, 181–190 (2022).
26. Bakatula, E. N., Richard, D., Neculita, C. M. & Zagury, G. J. Determination of point of zero charge of natural organic materials. *Environ. Sci. Pollut. Res.* **25**, 7823–7833 (2018).
27. Morales Urrea, D. A., Haure, P. M., García Einschlag, F. S. & Contreras, E. M. Horseradish peroxidase-mediated decolourization of Orange II: Modelling hydrogen peroxide utilization efficiency at different pH values. *Environ. Sci. Pollut. Res.* **25**, 19989–20002 (2018).
28. Ismadji, S., Soetaredjo, F. E. & Ayucitra, A. *Clay Materials for Environmental Remediation* (Springer, Cham, 2015).
29. Jin, X., Yu, B., Chen, Z., Arocena, J. M. & Thring, R. W. Adsorption of Orange II dye in aqueous solution onto surfactant-coated zeolite: Characterization, kinetic and thermodynamic studies. *J. Colloid Interface Sci.* **435**, 15–20 (2014).
30. Kali, A. *et al.* Efficient adsorption removal of an anionic azo dye by lignocellulosic waste material and sludge recycling into combustible briquettes. *Colloids Interfaces* **6**, 22 (2022).
31. Gupta, N., Kushwaha, A. K. & Chattopadhyaya, M. C. Application of potato (Solanum tuberosum) plant wastes for the removal of methylene blue and malachite green dye from aqueous solution. *Arab. J. Chem.* **9**, S707–S716 (2016).
32. Morales Urrea, D. A., Haure, P. M. & Contreras, E. M. Monitoring the enzymatic oxidation of xenobiotics by hydrogen peroxide through oxidation-reduction potential measurements. *Ind. Eng. Chem. Res.* **57**, 16518–16525 (2018).
33. Barakat, M. F., El-Salamawy, K., El-Banna, M., Abdel-Hamid, M. & Abdel-Rehim Taha, A. Radiation effects on some dyes in non-aqueous solvents and in some polymeric films. *Radiat. Phys. Chem.* **61**, 129–136 (2001).
34. Blümel, S., Knackmuss, H. J. & Stolz, A. Molecular cloning and characterization of the gene coding for the aerobic Azoreductase from *Xenophilus azovorans* KF46F. *Appl. Environ. Microbiol.* **68**, 3948–3955 (2002).
35. Zaini, M. A. A., Alias, N. & Yunus, M. A. C. Bio-polishing sludge adsorbents for dye removal. *Polish J. Chem. Technol.* **18**, 15–21 (2016).

36. Suresh Kumar, P. *et al.* Understanding and improving the reusability of phosphate adsorbents for wastewater effluent polishing. *Water Res.* **145**, 365–374 (2018).
37. Oakes, J. & Gratton, P. Kinetic investigations of azo dye oxidation in aqueous media. *J. Chem. Soc. Perkin Trans.* **2**, 1857–1864. https://doi.org/10.1039/a803892i (1998).
38. Febrianto, J. *et al.* Equilibrium and kinetic studies in adsorption of heavy metals using biosorbent: A summary of recent studies. *J. Hazard. Mater.* **162**, 616–645 (2009).
39. Ferro Orozco, A. M., Contreras, E. M. & Zaritzky, N. E. Dynamic response of combined activated sludge-powdered activated carbon batch systems. *Chem. Eng. J.* **157**, 331–338 (2010).
40. Mendes, P. GEPASI: A software package for modelling the dynamics, steady states and control of biochemical and other systems. *Bioinformatics* **9**, 563–571 (1993).
41. Mendes, P. & Kell, D. Non-linear optimization of biochemical pathways: Applications to metabolic engineering and parameter estimation. *Bioinformatics* **14**, 869–883 (1998).
42. Richhariya, G. & Kumar, A. Fabrication and characterization of mixed dye: Natural and synthetic organic dye. *Opt. Mater. (Amst)* **79**, 296–301 (2018).
43. Zhou, Y., Lu, J., Zhou, Y. & Liu, Y. Recent advances for dyes removal using novel adsorbents: A review. *Environ. Pollut.* **252**, 352–365 (2019).
44. Kao, C. M., Chou, M. S., Fang, W. L., Liu, B. W. & Huang, B. R. Regulating colored textile wastewater by 3/31 wavelength admi methods in Taiwan. *Chemosphere* **44**, 1055–1063 (2001).
45. Hemalatha, H. N. & Sanjay, N. C. S. Real silk textile wastewater treatment using 2-D electrochemical coagulation and estimation of electrical energy consumption. *Braz. J. Chem. Eng.* **40**, 151–158 (2023).

Acknowledgements

Author contributions

Conceptualization, methodology, and investigation were performed by D.M.-U., and A.L.-C. Formal analysis and writing—original draft preparation were performed by D.M.-U., A.L.-C, and E.M.C. Funding acquisition was carried out by A.L.-C. Resources, and project administration were carried out by A.L.-C. Writing—review and editing, visualization, supervision were performed by D.A.M.-U., E.M.C. , and A.L.-C. All authors have read and agreed to the published version of the manuscript.

Funding

Competing interests

The authors declare no competing interests.

Additional information

Supplementary Information The online version contains supplementary material available at https://doi.org/10.1038/s41598-024-70690-2.

Correspondence and requests for materials should be addressed to D.M.-U.

Reprints and permissions information is available at www.nature.com/reprints.

Publisher's note Springer Nature remains neutral with regard to jurisdictional claims in published maps and institutional affiliations.